

Improved thermoelectric performance of highly-oriented nanocrystalline bismuth antimony telluride thin films

Masayuki Takashiri ^{1,4}, Saburo Tanaka ², Koji Miyazaki ³

¹ Research Division, Komatsu Ltd., 1200 Manda, Hiratsuka, Kanagawa 254-8567, Japan

² Department of Biological Functions and Engineering, Kyushu Institute of Technology, 2-4 Hibikino, Wakamatsu-ku, Kitakyushu 808-0196, Japan

³ Department of Mechanical Engineering, Kyushu Institute of Technology, 1-1 Sensui, Tobata-ku, Kitakyushu 804-8550, Japan

E-mail: masayuki_takashiri@komatsu.co.jp

Abstract

Improved thermoelectric performance of highly-oriented nanocrystalline bismuth antimony telluride thin films is described. The thin films are deposited by a flash evaporation method, followed by annealing in hydrogen. By optimizing the annealing conditions, the resulting thin films exhibit almost perfect orientation with the c-axis normal to the substrate, and are composed of nano-sized grains with an average grain size of 150 nm. The in-plane electrical conductivity and Seebeck

coefficient were measured at room temperature. The cross-plane thermal conductivity of the thin films was measured by a 3ω method, and the in-plane thermal conductivity was evaluated by using an anisotropic factor of thermal conductivity based on a single crystal bulk alloy with almost the same composition and carrier concentration. The measured cross-plane thermal conductivity is 0.56 W/(m K), and the in-plane thermal conductivity is evaluated to be 1.04 W/(m K). Finally, the in-plane power factor and figure-of-merit, ZT , of the thin films are $35.6 \mu\text{W}/(\text{cm K}^2)$ and 1.03 at 300 K, respectively.

⁴ Author to whom any correspondence should be addressed

1. Introduction

There has been growing interest in nanostructured materials because of their attractive properties, which can differ from those of the corresponding bulk materials. Such differences are especially desirable in thermoelectric materials because of the potential of enhancing their performance by nanostructuring them, owing to the quantum confinement effect [1]. The performance of thermoelectric materials is characterized by the dimensionless figure-of-merit, ZT , defined as $ZT = S^2\sigma T/\kappa$, where S is the Seebeck coefficient, σ is the electrical conductivity, T is the absolute temperature and κ is the total thermal conductivity with contributions from the lattice (κ_L) and electrons (κ_e). The product $S^2\sigma$ is defined as the power factor. To obtain thermoelectric materials with high performance, the power factor needs to be maximized and the thermal conductivity minimized.

There have been persistent efforts to improve ZT of materials, and several groups have reported higher ZT values in superlattices since the lattice thermal conductivities (κ_L) are lower than those of the corresponding materials [2-4]. Though superlattices have achieved higher performance, it is a challenge to reduce production costs, since the deposition equipment and starting materials are expensive. From the viewpoint of industrial applications, it is desirable for thermoelectric materials to exhibit high performance near room temperature with low fabrication cost.

Recently, nanocrystalline bismuth antimony telluride bulk alloys fabricated by a conventional hot-pressing method yielded a ZT value of 1.4 at 373 K, which is a significantly improved thermoelectric performance compared to the bulk materials around room temperature [5]. This ZT

improvement may be responsible for the lower thermal conductivity caused by phonon scattering on grain boundaries. A reduction in thermal conductivity owing to the nanocrystalline grains has also been observed in bismuth-telluride based thin films [6-9].

For further improvement in the thermoelectric performance of bismuth-telluride based alloys, our strategy is to combine the nanostructure with high crystal orientation. The crystal structure of bismuth-telluride based alloys has been described as a rhombohedral tetradymite-type structure, and is known to exhibit high thermoelectric performance along the basal plane (a-b axis) [10]. In addition, carrier flow in most thin film thermoelectric devices is in the in-plane direction [11-13]. If the nanocrystals have a basal plane parallel to the in-plane direction, they are expected to achieve higher thermoelectric performance in this direction. In our previous study, we fabricated p-type nanocrystalline bismuth antimony telluride thin films with high orientation by a flash evaporation method with optimized annealing conditions, and showed lower thermal conductivity in the cross-plane direction compared to the single crystal bulk alloys for the mostly same atomic composition [14]. However, we did not report the thermoelectric performance of the thin films because the in-plane electrical properties were not measured, and the in-plane thermal conductivity was still not calculated.

In this work, we report improved performance of p-type highly-oriented nanocrystalline bismuth antimony telluride thin films formed by a flash evaporation method with an optimized annealing condition. First, the structural properties, including crystallinity, crystal orientation, grain size and atomic composition, were investigated. Then, the in-plane electrical conductivity and

Seebeck coefficient, were measured at room temperature. The cross-plane thermal conductivity was measured by a 3ω method, and the in-plane thermal conductivity was evaluated by using an anisotropic factor of thermal conductivity based on a single crystal bulk alloy with mostly the same composition and carrier concentration. Finally, we estimated the power factor and the figure-of-merit, ZT, in the in-plane direction.

2. Experimental

P-type bismuth antimony telluride thin films were fabricated on glass substrates (size: 50 mm × 50 mm, 1.1 mm thick) using a flash evaporation method. The detailed experimental setup has been described elsewhere [15,16]. Briefly, the starting material for the flash evaporation was spherical-shaped bismuth antimony telluride powder with an average powder size of 200 μm prepared by a centrifugal atomization method [17]. Inside the flash evaporation chamber, the distance between the tungsten boat and the substrate was 200 mm. When the chamber was evacuated to 1.4×10^{-3} Pa, a current of 80 A was applied to the tungsten boat until the substrate temperature reached 200 °C. By tilting the powder vessel gradually, the powders were fed on to the tungsten boat, which evaporated them on the glass substrate. The thickness of the thin films was approximately 190 nm. Next, hydrogen annealing was carried out. The samples were placed in an electric furnace that was evacuated to 1.0 Pa, which was purged five times with high-purity (99.999%) argon gas. The furnace was then filled with hydrogen gas at atmospheric pressure, with the hydrogen gas flow rate maintained

at 0.3 SLM throughout the annealing process. The temperature was increased steadily at a rate of 5 K/min to 300 °C, and the samples were then annealed at this temperature for 0 (as-deposited), 30 and 60 min. The annealing temperature of 300 °C was chosen because it yielded the highest performance for the power factor in our previous study [16]. After annealing, the samples were cooled naturally to room temperature. Finally, the adhesion of the samples was checked by a tape delamination test in order to confirm that the thin films had good contact with the substrate.

The crystallinity and orientation of the thin films were analyzed by x-ray diffraction (XRD). The surface grain structure was investigated using scanning electron microscopy (SEM). The atomic composition was estimated by energy dispersive x-ray spectroscopy (EDX).

The in-plane electrical conductivity of the thin films was measured at room temperature by a 4-point probe method with an accuracy of $\pm 3\%$. The in-plane Seebeck coefficient was also measured at room temperature with an accuracy of $\pm 5\%$. For this, one end of the thin film was connected to a heat sink and the other end to a heater. The Seebeck coefficient was determined as the ratio of the potential difference along the film to the temperature difference. The cross-plane thermal conductivity was determined at room temperature by the 3ω method with an accuracy of $\pm 10\%$ [18]. Details of the thermal conductivity measurement and the sample fabrication process for the 3ω method have been described in previous publications [19-21]. In brief, an SiO₂ film (700 nm thick) was deposited on the bismuth antimony telluride thin film at a low deposition rate (0.12 nm/sec) by a sputtering method. A thin aluminum wire was deposited on the sample by electron beam evaporation through shadow masks.

The thin aluminum wire was 20 μm wide and the length of the heater part was 2 mm. We also fabricated reference samples that lack the bismuth antimony telluride thin film but were otherwise identical to the primary samples. The reference samples were used to subtract the thermal properties of the insulation layer.

3. Results

3.1 Structural properties of bismuth antimony telluride thin films

The surface structure of the p-type bismuth antimony telluride thin films was investigated by means of SEM (figure 1). The SEM micrographs indicated that voids or holes were not presented in all the thin films in this study, and clearly show grain size differences. The crystal grains of the as-deposited thin film are very small compared to those of the annealed thin films, and the grain size was observed to be less than 50 nm. For an annealing time of 30 min, we confirmed nearly hexagonal-shaped crystals with grain sizes up to 200 nm. As the annealing time increased to 60 min, the crystalline grains of the thin films grew further to a maximum grain size of approximately 300 nm. We also observed topographic steps and terraces on the surface of the crystal grains.

The crystallinity and orientation of the bismuth antimony telluride thin films were investigated by XRD (figure 2). The XRD intensity of the thin films was enhanced as the annealing time increased, indicating that the crystallinity of the thin films became higher. With regards to the crystal orientation of the thin films, the XRD patterns of all the thin films in this study were found to

mostly exhibit c-axis oriented peaks. This shows that the thin films are highly oriented along the c-axis. Therefore, we note that the in-plane and cross-plane directions are identical with the a-b-axis (basal plane) and c-axis, respectively. Detailed analysis of the crystal orientation of the thin films is presented later in this paper.

Figure 3 shows the annealing time dependence of the structural properties of the p-type bismuth antimony telluride thin films in terms of the average grain size, the crystal orientation, and the atomic composition. The average grain size of the thin films was estimated from the full width at half maximum (FWHM) of the XRD peaks using Scherrer's equation, as shown in figure 3(a). The average grain size of the as-deposited thin film was 25 nm, and the crystal grains grew linearly as the annealing time increased. The average grain size of the thin films annealed for 30 min and 60 min was 90 nm and 150 nm, respectively.

The detailed crystal orientation of the thin films was estimated by the diffracted intensity ratio of the sum of all the c-axis oriented peaks, $\Sigma\{0\ 0\ 1\}$, to the sum of all of the peaks, $\Sigma\{h\ k\ l\}$, as shown in figure 3(b). The ratio of the as-deposited thin film was 0.96, which indicates the thin film already has relatively high orientation along the c-axis without the annealing process. After annealing for 30 and 60 min, the ratios were further enhanced to 0.98 and 0.99, respectively. We can consider that the annealed thin films have almost perfect orientation along the c-axis.

EDX yielded the atomic composition of the bismuth antimony telluride thin films, as shown in figure 3(c). The ratio of the atomic composition of the starting powders was Bi : Sb : Te = 8 : 30 :

62, and all of thin films in this study exhibited approximately the same composition as the starting powders, indicating that all the thin films are essentially stoichiometric.

3.2 In-plane electrical properties of bismuth antimony telluride thin films

The annealing time dependence of the in-plane electrical properties of p-type bismuth antimony telluride thin films, in terms of the electrical conductivity, Seebeck coefficient, and the power factor, are shown in figure 4. The in-plane electrical conductivity was enhanced with increasing annealing time (figure 4(a)). The electrical conductivity of the thin film annealed for 60 min is 6.4×10^4 S/m, which is approximately 4 times larger than that of the as-deposited thin film.

The in-plane Seebeck coefficient of the as-deposited thin film is $191 \mu\text{V/K}$, and is enhanced by the annealing treatment (figure 4(b)). The Seebeck coefficient of the annealed thin films for 30 and 60 min yielded similar values, and the maximum Seebeck coefficient was $252 \mu\text{V/K}$ at an annealing time of 30 min.

The correlation between the annealing time dependence of the electrical conductivity and the Seebeck coefficient is complicated. It is easy to understand the case where the electrical conductivity increased and the Seebeck coefficient was maintained constant as the annealing time increased. This is because mobility is enhanced by reducing carrier scattering on the grain boundaries as the grains grow while the carrier concentration is kept constant. However, our results show a different phenomenon. This may be because a large number of defects exist at the grain boundaries in the as-deposited thin film.

The defects act as acceptors so that the carrier concentration is increased but the Seebeck coefficient is decreased, while at the same time the mobility is decreased by carrier scattering at the grain boundaries. Thus, we suggest that the electrical conductivity of the as-deposited thin film remains relatively low because the influence of the reduced mobility surpasses its increased carrier concentration. On the other hand, the Seebeck coefficient of the thin films annealed for 30 and 60 min has similar values, while the electrical conductivity increased as the annealing time increased because most of the defects at the grain boundaries may already have vanished by the 30 min-annealing treatment, and only grain growth occurs due to the extended annealing time.

The in-plane power factor is significantly improved by the annealing treatment (figure 4(c)). The power factor of the as-deposited thin film is $5.4 \mu\text{W}/(\text{cm}\cdot\text{K}^2)$, and it increased to $34.9 \mu\text{W}/(\text{cm}\cdot\text{K}^2)$ for the annealing time of 30 min. Finally, the power factor reached $35.6 \mu\text{W}/(\text{cm}\cdot\text{K}^2)$ at the annealing time of 60 min.

3.3 Cross-plane thermal conductivity of bismuth antimony telluride thin films

For measuring the cross-plane thermal conductivity of p-type bismuth antimony telluride thin films, we used the thin film sample that was annealed for 60 min since it exhibited the highest crystal orientation ($\Sigma\{0\ 0\ 1\}/\Sigma\{h\ k\ l\}=0.99$) and power factor ($S^2\sigma = 35.6 \mu\text{W}/(\text{cm}\cdot\text{K}^2)$) in addition to having nano-sized crystal grains (average grain size = 150 nm). Figure 5 shows experimentally measured temperature amplitudes by a 20 μm wide heater on both the reference sample and the bismuth antimony

telluride thin film sample. The inset in figure 5 shows the sample configuration for the thermal conductivity measurement by the 3ω method. The width of the heater is significantly larger than the sum of the thickness of the bismuth antimony telluride thin film and the SiO_2 film, so that the direction of heat flow can be considered to be perpendicular to the thin film. Therefore, the measured thermal conductivity corresponds to the cross-plane direction. The thermal conductivity of the thin film is extracted from curve fitting of the measured temperature difference [22-24]. As a result, the cross-plane thermal conductivity of the thin film was determined to be 0.56 W/(m K) .

We compared the cross-plane thermal conductivity of the highly-oriented nanocrystalline bismuth antimony telluride thin film to that of the single crystal bulk alloy with nearly the same composition and carrier concentration [10]. The thermal conductivity of the thin film is 20% smaller than that of corresponding single crystal bulk alloy. We previously reported the dependence of the lattice thermal conductivity on the grain size of Bi_2Te_3 thin films based on experimental results and the theory of phonon scattering on grain boundaries [6]. This report indicated that enhanced phonon scattering due to the nanocrystalline structure of the thin film is responsible for the observed reduction in thermal conductivity. Because of this, the mechanism of reduced thermal conductivity in the case of the Bi_2Te_3 thin films can be applied to the bismuth antimony telluride thin films.

4. Discussion

We present the in-plane thermoelectric properties of the p-type bismuth antimony telluride thin

films because this direction is the most important one for thermoelectric thin film devices. In this study, the electrical conductivity and Seebeck coefficient in the in-plane direction were measured, and the thermal conductivity was measured in the cross-plane direction.

In order to evaluate the in-plane figure-of-merit of the thin film, we first estimated the in-plane thermal conductivity from the measured cross-plane thermal conductivity, the calculated in-plane electronic thermal conductivity and the anisotropic factor of thermal conductivity based on the single crystal bulk alloy with mostly the same composition and carrier concentration, as shown in table 1. The measured cross-plane thermal conductivity was determined to be 0.56 W/(m K) by the 3ω method. The in-plane electronic thermal conductivity was calculated to be 0.47 W/(m K) using the Wiedemann-Franz law. We assume that the electronic anisotropic factor of the single crystal bulk alloy is the same as its highly-oriented nanocrystalline thin film because the average grain size is comparable in size to the film thickness. As a result, the cross-plane electronic thermal conductivity is estimated to be 0.15 W/(m K), and then the cross-plane lattice thermal conductivity is automatically determined to be 0.41 W/(m K) by subtracting the cross-plane electronic thermal conductivity from the total thermal conductivity. For estimating the in-plane lattice thermal conductivity with more accuracy, we need to use the model of phonon scattering on the grain boundaries. However, for a preliminary estimation in this study, we evaluated the in-plane lattice thermal conductivity by assuming that the lattice anisotropic factor of the single crystal bulk alloy is the same as its highly-oriented nanocrystalline thin film. As a result, the in-plane lattice thermal conductivity was

evaluated to be 0.57 W/(m K). The in-plane total thermal conductivity was determined to be 1.04 W/(m K) by adding the in-plane electronic thermal conductivity and the lattice thermal conductivity.

The in-plane thermoelectric properties of the highly-oriented nanocrystalline bismuth antimony telluride thin film and related materials are shown in table 2 [8,10,25]. The in-plane power factor of the highly-oriented nanocrystalline thin film is comparable to that of the well-established thin films fabricated by pulsed laser deposition (PLD) and metalorganic chemical vapor deposition (MOCVD), and approximately 10% lower than that of the single crystal bulk alloy.

The in-plane figure-of-merit, ZT , of the highly-oriented nanocrystalline thin film possibly reaches 1.03, which is approximately 20% higher than that of the single crystal bulk alloy. We consider that this enhancement in ZT is largely due to the lower thermal conductivity of the thin film. Therefore, though our estimation of ZT includes several assumptions, we may conclude that the thin film with high-orientation and nano-sized crystals is effective for improving thermoelectric performance.

5. Conclusions

We have reported improved performance of p-type highly-oriented nanocrystalline bismuth antimony telluride thin films by the flash evaporation method with an optimized annealing condition. The crystallinity and crystal orientation were enhanced as the annealing time increased. At an annealing time of 60 min, the thin film was composed of fine crystal grains with an average grain size

of 150 nm, with high crystallinity and crystal orientation along the c-axis with the diffracted intensity ratio, $\Sigma\{0\ 0\ l\}/\Sigma\{h\ k\ l\}$, of 0.99, which is almost perfect orientation. The atomic composition of the thin film was essentially stoichiometric. The in-plane electrical properties were also enhanced by the annealing treatment. The in-plane power factor of the thin film annealed for 60 min reached 35.6 $\mu\text{W}/(\text{cm K}^2)$, comparable to that of well-established thin films fabricated using well-known methods. The cross-plane thermal conductivity measured by the 3ω method was determined to be 0.56 $\text{W}/(\text{m K})$. The thermal conductivity of the thin film was 20% smaller than the corresponding single crystal bulk alloy owing to enhanced phonon scattering by the nanocrystalline structure. Finally, we evaluated the dimensionless figure-of-merit, ZT , in the in-plane direction since this direction is the most important for thermoelectric thin film devices, and determined ZT to be 1.03 at 300 K. Therefore, though our estimation of ZT includes several assumptions, we may conclude that thin films with high-orientation and nano-sized crystals are effective for improvement of thermoelectric performance.

Acknowledgments

The authors wish to thank Prof. Tsukamoto at Kitakyushu National College of Technology for his continuous encouragement, Prof. Dames at the University of California, Riverside, for valuable comments, and Dr. Jacquot at Fraunhofer Institut Physikalische Messtechnik in Germany for experimental support.

References

- [1] Hicks L D and Dresselhaus M S 1993 *Phys. Rev. B* **47** 12727
- [2] Venkatasubramanian R, Siivola E, Colpitts T and O'Quinn B 2001 *Nature* **413** 597
- [3] Harman T C, Taylor P J, Walsh M P and LaForge B E 2002 *Science* **297** 2229
- [4] Beyer H, Nurnus J, Böttner H, Lambrecht A, Roch T and Bauer G 2002 *Appl. Phys. Lett.* **80** 1216
- [5] Poudel B, Hao Q, Ma Y, Lan Y, Minnich A, Yu B, Yan X, Wang D, Muto A, Vashaee D, Liu J, Dresselhaus M S, Chen G and Ren Z 2008 *Science* **320** 634
- [6] Takashiri M, Miyazaki K, Tanaka S, Kurosaki J, Nagai D and Tsukamoto H 2008 *J. Appl. Phys.* **104** 084302
- [7] Liao C N, Wang Y C and Chu H S 2008 *J. Appl. Phys.* **104** 104312
- [8] Obara H, Higomo S, Ohta M, Yamamoto A, Ueno K and Iida T 2009 *Jpn. J. Appl. Phys.* **48** 085506
- [9] Chiritescu C, Mortensen C, Cahill D G, Johnson D and Zschack P 2009 *J. Appl. Phys.* **106** 073503
- [10] Rowe D M 1995 *CRC Handbook of Thermoelectrics* (London: CRC Press) chapter 19
- [11] Takashiri M, Shirakawa T, Miyazaki K and Tsukamoto H 2007 *Sens Actuators A* **138** 329
- [12] Goncalves L M, Rocha J G, Couto C, Alpuim P, Min G, Rowe D M and Correia J H 2007 *J. Micromech. Microeng.* **17** 168
- [13] Qiu F, Shin W, Matsumiya M, Izu N, Matsubara I and Murayama N 2004 *Sens Actuators B* **103** 252
- [14] Takashiri M, Tanaka S, Miyazaki K and Tsukamoto H 2010 *J. Alloys Compd.* (in press)

- [15] Takashiri M, Shirakawa T, Miyazaki K and Tsukamoto H 2007 *J. Alloys Compd.* **441** 246
- [16] Takashiri M, Miyazaki K and Tsukamoto H 2008 *Thin Solid Films* **516** 6336
- [17] Kajihara T, Konishi A, Lee Y H, Sasaki K, Tomita K and Kajiura T 2001 *Japan Patent*
P2001-320097
- [18] Takashiri M, Borca-Tasciuc T, Jacquot A, Miyazaki K and Chen G 2006 *J. Appl. Phys.* **100** 54315
- [19] Borca-Tasciuc T, Kumar A R and Chen G 2001 *Rev. Sci. Instrum.* **72** 2139
- [20] Jacquot A, Lenoir B, Dauscher A, Stölzer M and Meusel J 2002 *J. Appl. Phys.* **91** 4733
- [21] Takashiri M, Takiishi M, Tanaka S, Miyazaki K and Tsukamoto H 2007 *J. Appl. Phys.* **101** 074301
- [22] Cahill D G 1990 *Rev. Sci. Instrum.* **61** 802
- [23] Cahill D G, Katiyar M and Abelson J R 1994 *Phys. Rev. B* **50** 6077
- [24] Ju Y S, Kurabayashi K and Goodson K E 1999 *Thin Solid Films* **339** 160
- [25] Mzerd A, Aboulfarah B, Giani A and Boyer A 2006 *J. Mater. Sci.* **41** 1659

Tables

Table 1. The total, electronic and lattice thermal conductivities of the highly-oriented nanocrystalline bismuth antimony telluride thin film and related material. The superscripts, a, b and c indicate the thermal conductivities measured respectively by the 3ω method, estimated from the Weidemann-Franz law and the anisotropic factor.

Sample structure	Direction	Orientation $\Sigma(00l)/\Sigma(hkl)$	Grain size (nm)	κ_{total}	κ_e (W/m K)	κ_L	$\frac{\kappa_e \text{ (in-plane)}}{\kappa_e \text{ (cross-plane)}}$	$\frac{\kappa_L \text{ (in-plane)}}{\kappa_L \text{ (cross-plane)}}$	Ref.
Highly-oriented nanocrystalline thin film (annealing time: 60 min)	In-plane (a-b axis)	0.99	150	1.04 ^{b+c}	0.47 ^b	0.57 ^c	3.12	1.39	This work
	Cross-plane (c-axis)			0.56 ^a	0.15 ^c	0.41 ^{a-c}			
Single crystal bulk alloy	a-b axis	1.00		1.36	0.57	0.79	3.12	1.39	ref. 10
	c-axis			0.75	0.18	0.57			

Table 2. In-plane thermoelectric properties of the highly-oriented nanocrystalline bismuth antimony telluride thin film and related materials. The superscript * indicates the values estimated by using several assumptions.

Sample structure	Orientation $\Sigma(001)/\Sigma(hkl)$	Grain size (nm)	σ (10^4 S/m)	S (μ V/K)	σS^2 (μ W/cm K ²)	κ_{total} (W/m K)	ZT at 300K	Ref.
Highly-oriented nanocrystalline thin film (annealing time: 60 min)	0.99	150	6.4	236	35.6	1.04 *	1.03 *	This work
Single crystal bulk alloy	1.00		7.8	225	39.5	1.36	0.87	ref. 10
Bi _{0.3} Sb _{1.7} Te _{3.0} thin film by PLD	not mentioned		9.2	198	36.1	-	-	ref. 8
(Bi _{1-x} Sb _x) ₂ Te ₃ thin film by MOCVD	not mentioned		5.9	240	34.0	-	-	ref. 25

Figure captions

Figure 1. Surface structure of the bismuth antimony telluride thin films obtained using SEM, annealed for 0 min (as-deposited) (#1), 30 min (#2) and 60 min (#3)

Figure 2. XRD patterns of the bismuth antimony telluride thin films annealed for 0 min (as-deposited) (#1), 30 min (#2) and 60 min (#3).

Figure 3. Annealing time dependence of structural properties of the bismuth antimony telluride thin films. Average grain size is shown in (a), the crystal orientation in (b), and the atomic composition in (c). The inset in figure 3(c) is the atomic composition of the starting powders.

Figure 4. Annealing time dependence of the in-plane thermoelectric properties of the bismuth antimony telluride thin films. Electrical conductivity is shown in (a), the Seebeck coefficient in (b), and the thermoelectric power factor in (c).

Figure 5. The temperature amplitudes by 20 μm wide heaters deposited onto the reference and the bismuth antimony telluride thin film annealed for 60 min.

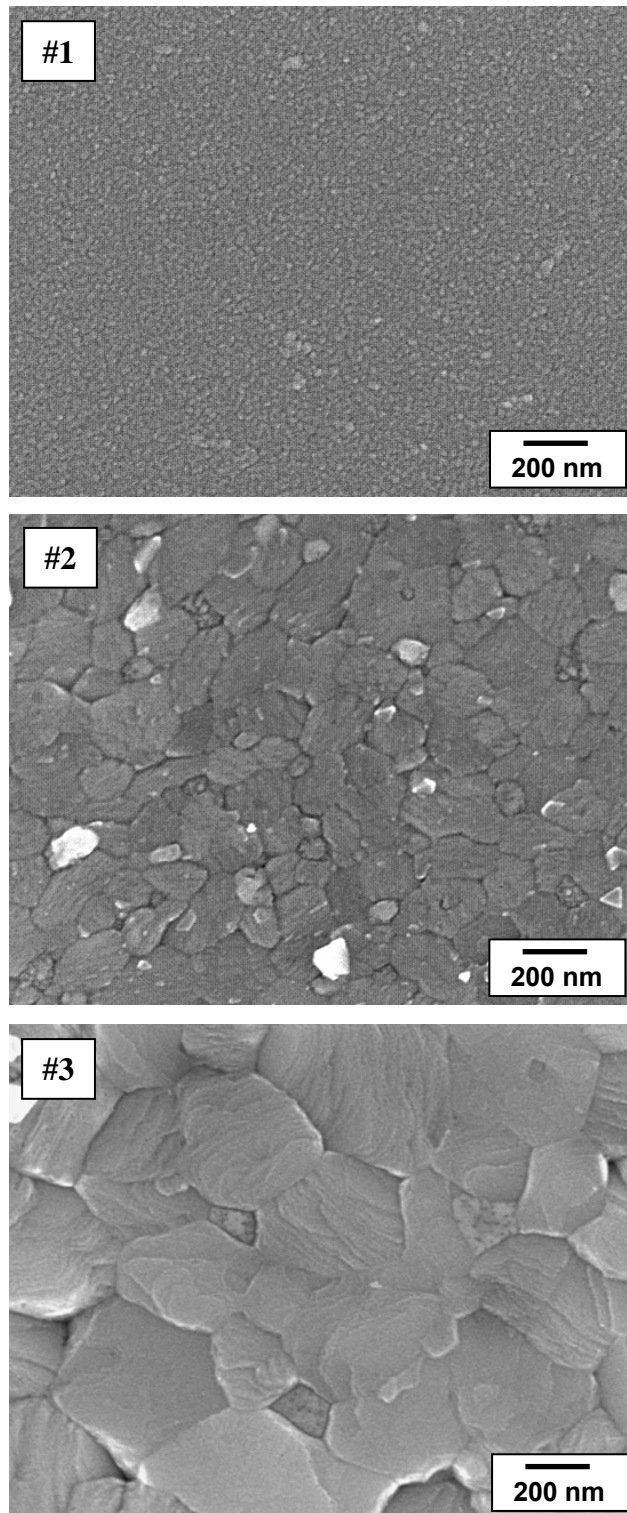


Figure 1

Surface structure of the bismuth antimony telluride thin films obtained using SEM, annealed for 0 min (as-deposited) (#1), 30 min (#2) and 60 min (#3)

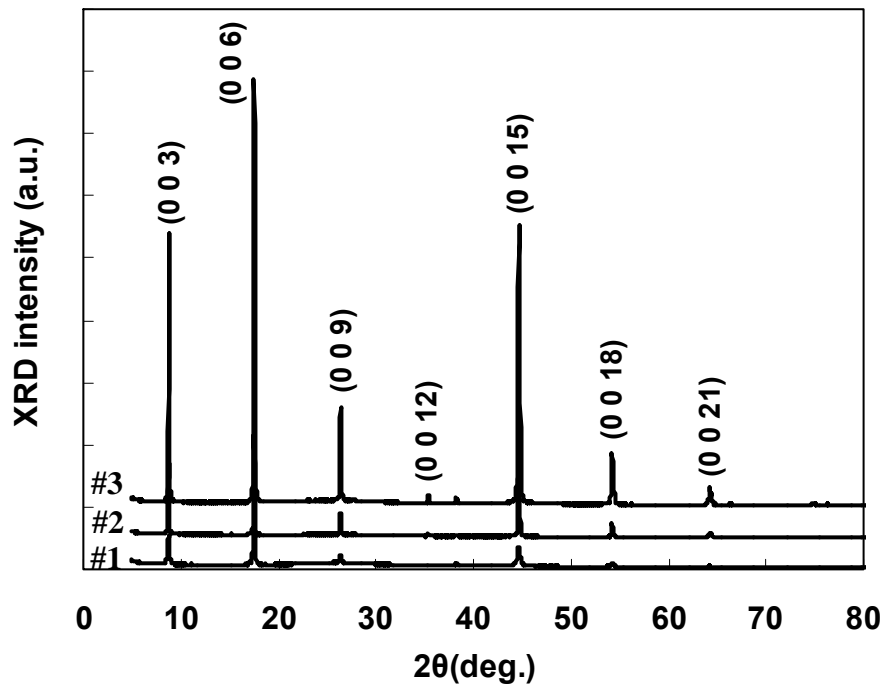


Figure 2

XRD patterns of the bismuth antimony telluride thin films annealed for 0 min (as-deposited) (#1), 30 min (#2) and 60 min (#3).

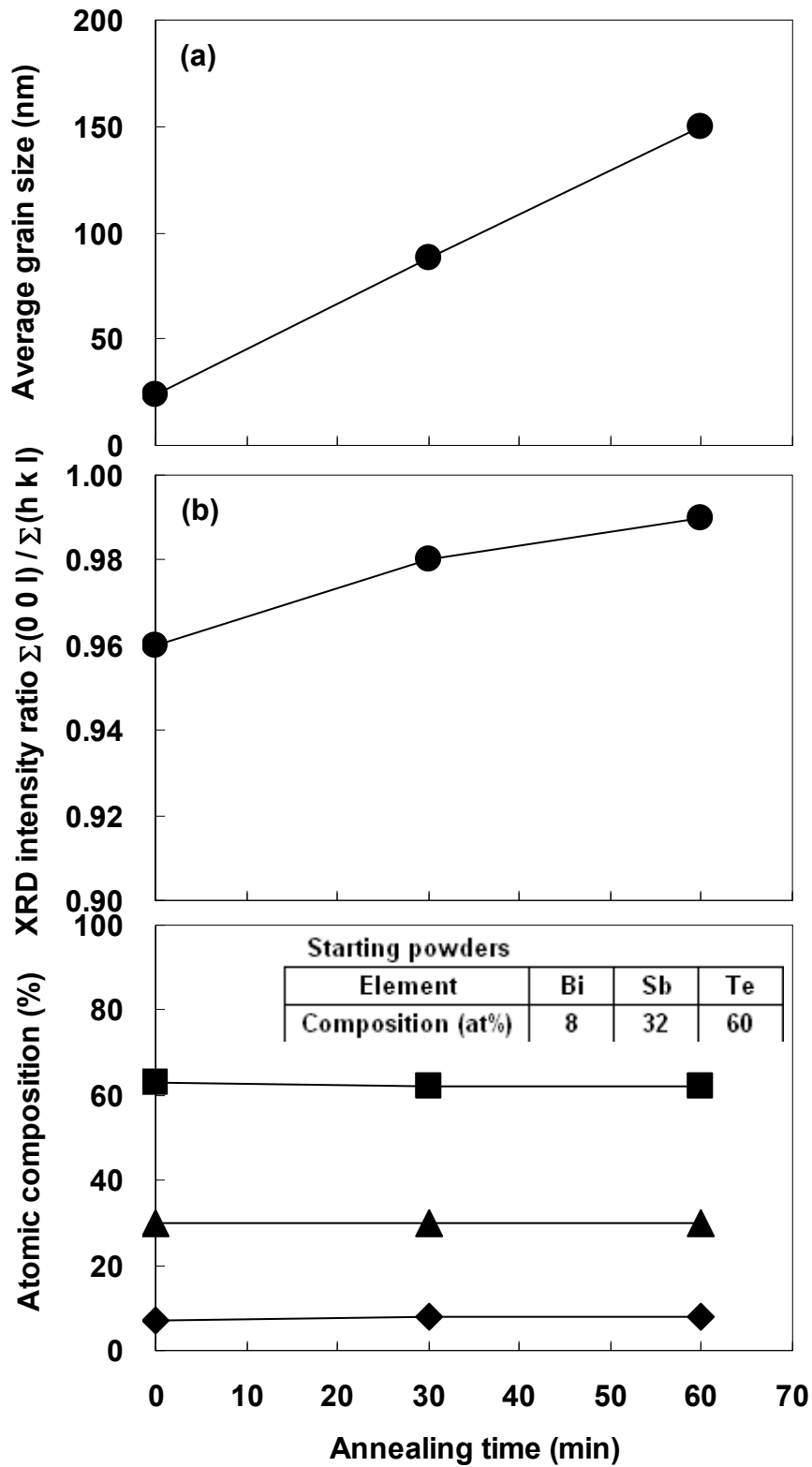


Figure 3

Annealing time dependence of structural properties on the bismuth antimony telluride thin films. Average grain size is shown in (a), crystal orientation in (b), atomic composition in (c). The inset of Fig.3 (c) is the atomic composition of the starting powders.

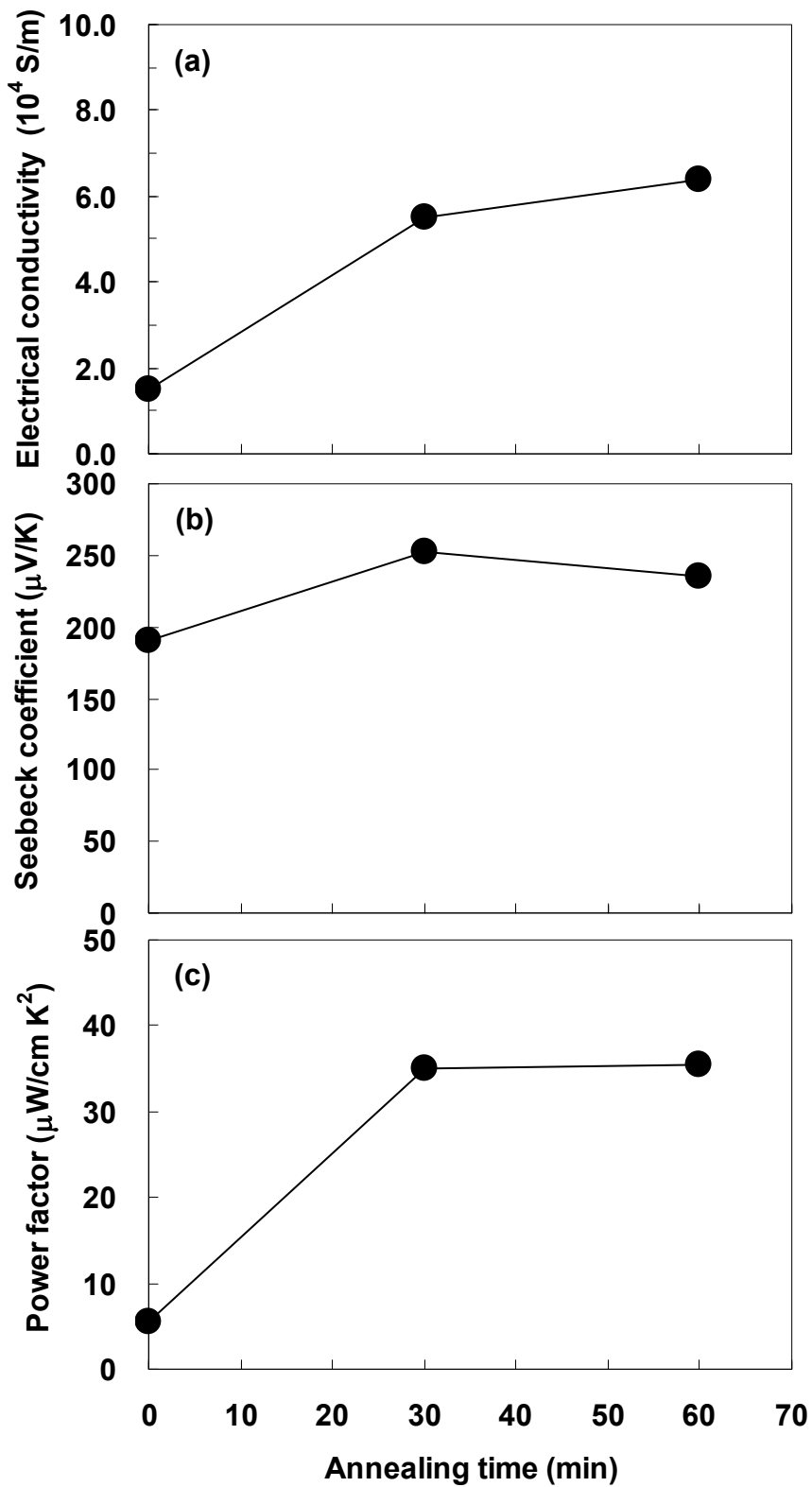


Figure 4

Annealing time dependence of the in-plane thermoelectric properties of the bismuth antimony telluride thin films. Electrical conductivity is shown in (a), Seebeck coefficient in (b), thermoelectric power factor in (c).

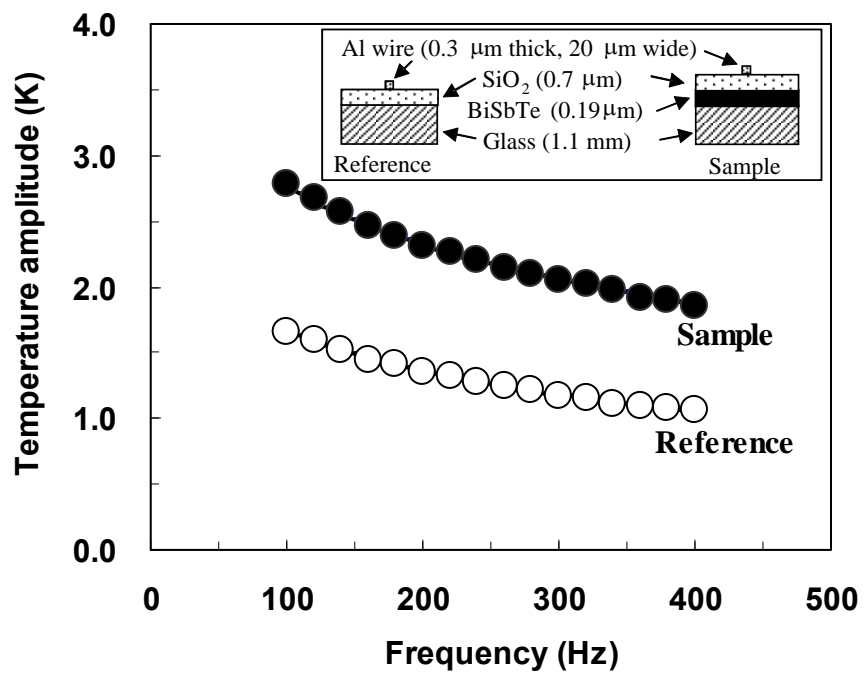


Figure 5

The temperature amplitudes by 20 μm wide heaters deposited onto the reference and the bismuth antimony telluride thin film annealed for 60 min.